

## Article

# Low-Temperature Hydrogenation of Toluene Using an Iron-Promoted Molybdenum Carbide Catalyst

Song Zhou <sup>1,2</sup>, Xi Liu <sup>3,4,\*</sup>, Jian Xu <sup>3,\*</sup> , Hui Zhang <sup>5</sup>, Xiaosong Liu <sup>5</sup>, Pengcheng Li <sup>6</sup>, Xiaodong Wen <sup>1,3</sup>, Yong Yang <sup>1,3</sup> and Yongwang Li <sup>1,3</sup>

- <sup>1</sup> State Key Laboratory of Coal Conversion, Institute of Coal Chemistry, Chinese Academy of Sciences, Taiyuan 030001, China; zhousong@sxicc.ac.cn (S.Z.); wenxiaodong@synfuelschina.com.cn (X.W.); yangyong@synfuelschina.com.cn (Y.Y.); liyongwang@synfuelschina.com.cn (Y.L.)
- <sup>2</sup> School of Chemistry and Chemical Engineering, University of Chinese Academy of Sciences, Beijing 100049, China
- <sup>3</sup> SynCat@Beijing, Synfuels China Technology Co. Ltd., Beijing 100049, China
- <sup>4</sup> In Situ Center for Physical Sciences, School of Chemistry and Chemical Engineering, Shanghai Jiao Tong University, Shanghai 200240, China
- <sup>5</sup> State Key Laboratory of Functional Materials for Informatics, Shanghai Institute of Microsystem and Information Technology, Chinese Academy of Sciences, Shanghai 200050, China; huizhang@mail.sim.ac.cn (H.Z.); xslu19@ustc.edu.cn (X.L.)
- <sup>6</sup> Luoyang R&D Center of Technology Sinopec Engineering (Group) Co., Ltd., Luoyang 471003, China; lipengcheng.segr@sinopec.com
- \* Correspondence: liuxi@sjtu.edu.cn (X.L.); xujian@synfuelschina.com.cn (J.X.)



**Citation:** Zhou, S.; Liu, X.; Xu, J.; Zhang, H.; Liu, X.; Li, P.; Wen, X.; Yang, Y.; Li, Y. Low-Temperature Hydrogenation of Toluene Using an Iron-Promoted Molybdenum Carbide Catalyst. *Catalysts* **2021**, *11*, 1079. <https://doi.org/10.3390/catal11091079>

Academic Editors: Andres Aguayo and Eva Bejerano

Received: 11 August 2021

Accepted: 4 September 2021

Published: 8 September 2021

**Publisher's Note:** MDPI stays neutral with regard to jurisdictional claims in published maps and institutional affiliations.



**Copyright:** © 2021 by the authors. Licensee MDPI, Basel, Switzerland. This article is an open access article distributed under the terms and conditions of the Creative Commons Attribution (CC BY) license (<https://creativecommons.org/licenses/by/4.0/>).

**Abstract:** As an alternative to noble metal hydrogenation catalysts, pure molybdenum carbide displays unsatisfactory catalytic activity for arene hydrogenation. Precious metals such as palladium, platinum, and gold are widely used as additives to enhance the catalytic activities of molybdenum carbide, which severely limits its potential applications in industry. In this paper, iron-promoted molybdenum carbide was prepared and characterized by various techniques, including in situ XRD, synchrotron-based XPS and TEM. While the influence of Fe addition on catalytic performance for toluene hydrogenation was also studied. The experimental data disclose that a small amount of Fe doping strongly enhances catalytic stability in toluene hydrogenation, but the catalytic performance drops rapidly with higher loading amounts of Fe.

**Keywords:** molybdenum carbide; Fe-promoter; toluene hydrogenation; synchrotron-based XPS; in situ XRD

## 1. Introduction

Catalytic hydrogenation of arenes has continuously received attention due to increasing demands for the production of synthetic textiles and other fine chemicals [1,2]. Meanwhile, iterative catalytic hydrogenation/dehydrogenation of arenes/corresponding naphthalene pairs has been used for hydrogen storage and transportation [3]. To convert stable molecules under mild conditions (for example, below 100 °C) with high selectivity and yield, noble metals such as platinum, ruthenium and rhodium are required as the main catalytic components in these processes [4–13]. Nevertheless, these catalysts have not received widespread industrial use because of their high cost, complex preparation procedures and vulnerability to sulfur poisoning [14–17]. On the other hand, cheaper supported Ni and Co catalysts including Ni-W/Al<sub>2</sub>O<sub>3</sub>, Co-Mo/Al<sub>2</sub>O<sub>3</sub>, Ni-Mo/Al<sub>2</sub>O<sub>3</sub> and other industrial catalysts, are less active for this hydrogenation reaction and must be operated under a high reaction temperature and pressure [6,18–27]. Transition metal carbide catalysts (molybdenum carbide, tungsten carbide, etc.) exhibit Pt-like characteristics in various reactions with excellent anti-poisoning properties [14,15,28,29]. In recent years, with the development of preparation methods, molybdenum carbide has been applied in the fields of CO

hydrogenation [30], ammonia synthesis [31,32], CO<sub>2</sub> hydrogenation [33–35], hydrodesulfurization (HDS), furfural hydrogenation [36] and hydrodenitrogenation (HDN) [37–40]. However, efforts focusing on the applications of carbide catalysts for arene hydrogenation have been limited. Furthermore, pure carbide materials exhibit lower catalytic activities and stabilities than platinum-like metals, and so the catalysts must be improved.

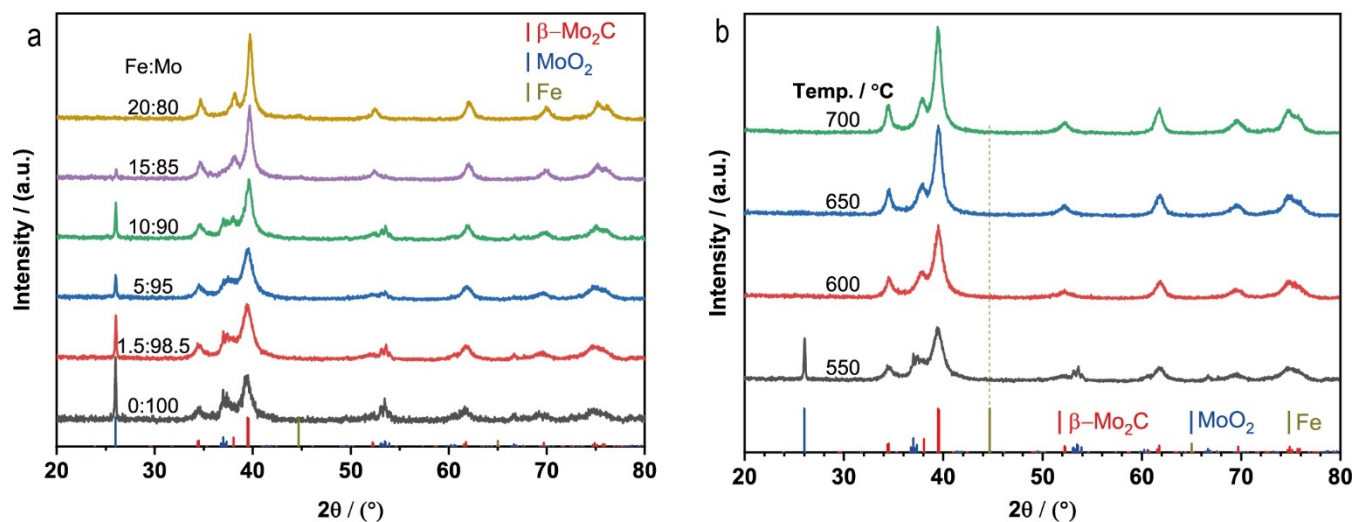
In most cases, catalytic performance of a given catalyst could be improved by doping transition metals, and noble metals are widely used as key additives to promote the catalytic performance of carbide catalysts [41], which inevitably increases the cost of the catalysts and consequently hinders their industrial applications [3,4,30,31,33,42,43]. It is of great industrial and academic interest to use inexpensive additives and develop preparation methods to achieve cheap and highly active catalysts. Numerous works have been undertaken doping base transition metals to molybdenum carbide. For instance, the molybdenum carbide as catalyst for conversion of CO<sub>2</sub> into ethylene was improved by doping Fe for tailoring its activity and stability [44], doping the base transition metals (Fe, Co, and Ni) to molybdenum carbide enhances the hydrogen evolution in mildly acidic and alkaline media [45], and the activity of CO hydrogenation was also modulated by doping transition metals (Fe, Co, and Ni) [46]. Therefore, we plan to use the base transition metal to improve the activity of toluene hydrogenation. The transition metal, Fe, has been reported to facilitate the toluene hydrogenation by using unsupported and supported Fe as catalysts [47,48]. Here, we would dope the molybdenum carbide with Fe to promote the catalytic performance by the interaction between Fe and the molybdenum carbides.

Therefore, we prepared Fe-promoting molybdenum carbide catalysts with different Fe loading amounts and carburization temperatures. The experimental results disclose that loaded Fe species are highly dispersed and largely exist on the surface of molybdenum carbide catalysts, which strongly enhance the catalytic activity and stability. However, the Fe-promoting Mo<sub>2</sub>C catalyst can be oxidized by trace amounts of oxygen species during the hydrogenation process, but the catalytic performance can fully recover after the recarburization process.

## 2. Results and Discussion

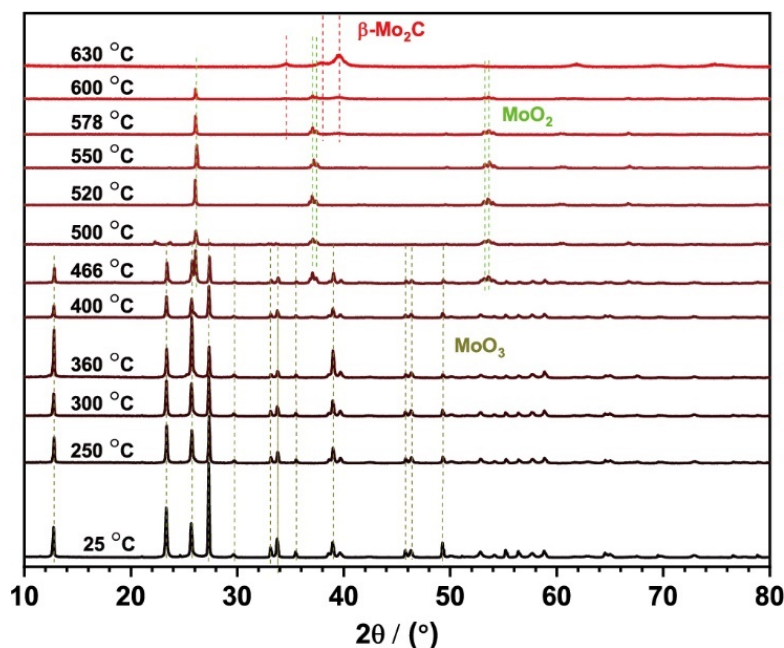
### 2.1. Physicochemical Properties and Morphology of the Fe/Mo<sub>2</sub>C Catalysts

Figure 1 shows XRD patterns of the Fe/Mo<sub>2</sub>C catalysts carburized at 550 °C with different Fe loadings (Fe:Mo molar ratios equal to 0:100, 1.5:98.5, 5:95, 10:90, 15:85, and 20:80, which are denoted as Mo<sub>2</sub>C-550, 1.5Fe-Mo<sub>2</sub>C-550, 5Fe-Mo<sub>2</sub>C-550, 10Fe-Mo<sub>2</sub>C-550, 15Fe-Mo<sub>2</sub>C-550 and 20Fe-Mo<sub>2</sub>C-550, respectively). The characteristic diffraction peaks located at 2θ of 34.8°, 38.4°, and 39.8° for the Fe-MoO<sub>3</sub> precursors are assigned to the hexagonal β-Mo<sub>2</sub>C phase (hcp crystal structure), while the characteristic diffraction peaks at 2θ of 26.0°, 37.0°, and 53.5° are attributed to the MoO<sub>2</sub> phase with a monoclinic crystal structure [49]. In the catalyst with 1.5 mol% Fe, the main component is β-Mo<sub>2</sub>C with a trace amount of MoO<sub>2</sub>. When the Fe/Mo molar ratio increases, the content of the MoO<sub>2</sub> phase steadily decreases until no MoO<sub>2</sub> is found in the carbide material with 15 or 20 mol% Fe. In comparison, the non-Fe-promoted catalyst contains much higher amounts of MoO<sub>2</sub> (also seen in Figure S1a), which suggests that the addition of Fe considerably promotes the carburization process. However, a small peak at 44.7° assigned to metallic Fe appears in the XRD patterns of the 15Fe-Mo<sub>2</sub>C-550 and 20Fe-Mo<sub>2</sub>C-550 catalysts, which should be attributed to the segregation of overloaded Fe species. Figure 1b shows that catalysts with an Fe/Mo molar ratio of 1.5/98.5 grew in crystallite size from 5.6 to 9.7 nm with increasing carburization temperatures. For the low Fe doping carbide catalysts, no characteristic diffraction peaks of metallic Mo and Fe were detected, indicating the good dispersion of Fe species in the bulk or surface.



**Figure 1.** X-ray diffraction (XRD) patterns of Fe-promoted molybdenum carbides (Fe/Mo<sub>2</sub>C-550) (a) with different Fe promoting amounts and 1.5Fe/Mo<sub>2</sub>C (b) with different final carburization temperatures.

Furthermore, an in situ XRD technique was used to study the phase transition during the preparation of the 1.5Fe-Mo<sub>2</sub>C-550 catalyst. As shown in Figure 2, the reduction and carburization of MoO<sub>3</sub> in 20%CH<sub>4</sub>/H<sub>2</sub> proceeded via two steps. First, the intensity of MoO<sub>3</sub> gradually decreased as the temperature increased from 25 °C to 460 °C, and MoO<sub>3</sub> was completely converted at approximately 500 °C; moreover, the formation of MoO<sub>2</sub> and Mo<sub>2</sub>C appeared at 466 °C and 578 °C, respectively. At 630 °C, all molybdenum oxides were converted to Mo<sub>2</sub>C. No molybdenum metal appeared during the MoO<sub>3</sub> and MoO<sub>2</sub> transitions, indicating that MoO<sub>2</sub> was directly transformed into molybdenum carbide and that no other intermediate phase formed. Nevertheless, Fe did not appear throughout the carburization process, which suggests that no aggregation-redispersion process occurs.



**Figure 2.** In situ XRD study of the carburization process of precursor 1.5Fe-MoO<sub>3</sub>.

## 2.2. Spatial Distribution of Fe-Promoter and Mo<sub>2</sub>C Phases in the Fe/Mo<sub>2</sub>C Catalysts

Microscopic evidence shown in Figure 3 confirm the synthesis of β-Mo<sub>2</sub>C with porous microstructure. Furthermore, we analyzed the element distributions of iron and molybde-

num in the fresh catalyst by the STEM-EDX mapping technique (Figure 3e). The distribution of Fe in the 1.5Fe-Mo<sub>2</sub>C-550 catalyst was highly uniform in the molybdenum carbide, which confirms that iron species exist as single atoms or extra small clusters in the carbide.

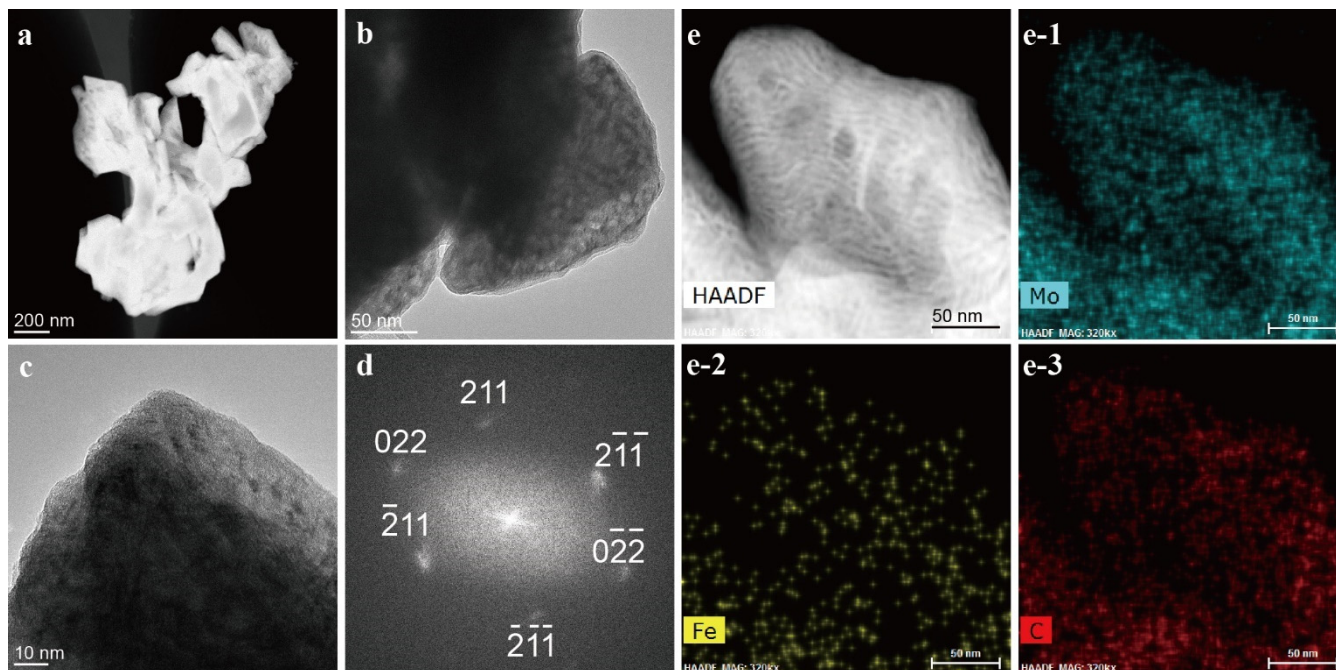


**Figure 3.** (a) High-angle annular dark-field scanning transmission electron microscopy (STEM-HAADF) image, and transmission electron microscopy (TEM) images (b,c) of the fresh 1.5Fe-Mo<sub>2</sub>C-550 catalyst, (d) corresponding fast Fourier transform (FFT) image confirming the presence of  $\beta$ -Mo<sub>2</sub>C, (e) STEM-HAADF and corresponding energy-dispersive X-ray spectroscopy (EDX) element mapping of (e-1) Mo, (e-2) Fe, (e-3) C of fresh catalyst 1.5Fe-Mo<sub>2</sub>C-550.

To reveal whether Fe is dispersed in the bulk or on the surface of catalysts, synchrotron-based XPS measurements were performed at BL02B of the Shanghai Synchrotron Radiation Facility (SSRF), with photon energies of 400, 900, and 1400 eV to generate photoelectrons. For Mo and C, 400, 900 and 1400 eV were used to excite photoelectrons from the Mo 3d and C 1s core levels, and the kinetic energies of the excited photoelectrons were about 150, 650, and 1150 eV, respectively. The inelastic mean free paths (IMFPs) of these emitted photoelectrons were about 0.5, 1.0 and 2.0 nm, respectively [50–52]. For Fe, photon energies of 900 and 1400 eV were chosen to excite Fe 2p core-level electrons with kinetic energies of about 150 and 650 eV, respectively. The inelastic mean free paths (IMFPs) of these emitted photoelectrons were about 0.5 and 1.0 nm, respectively. This choice confirmed that the kinetic energies (or IMFPs) of emitted photoelectrons from core levels of the compositional elements in the same catalyst were analogical. After calibration for the photon flux and cross section in photoemission, the measured intensities change provided compositional information as a function of depth of the Fe/Mo<sub>2</sub>C catalysts.

As shown in Figure 4a, the chemical states of Fe species at different depths are closer to metallic Fe but positively shift by approximately 0.6 eV, indicating electron transfer from Fe to molybdenum carbide [53]. The C 1s XPS spectra (Figure 4a) confirm that graphitic carbon partially deposits on the Mo<sub>2</sub>C surface with a thickness of approximately 0.5 nm, which should be attributed to the unexpected graphitization reaction occurring at high temperature. The Mo 3d binding energy peaked at 283.3 eV and remained unchanged at the different depths.

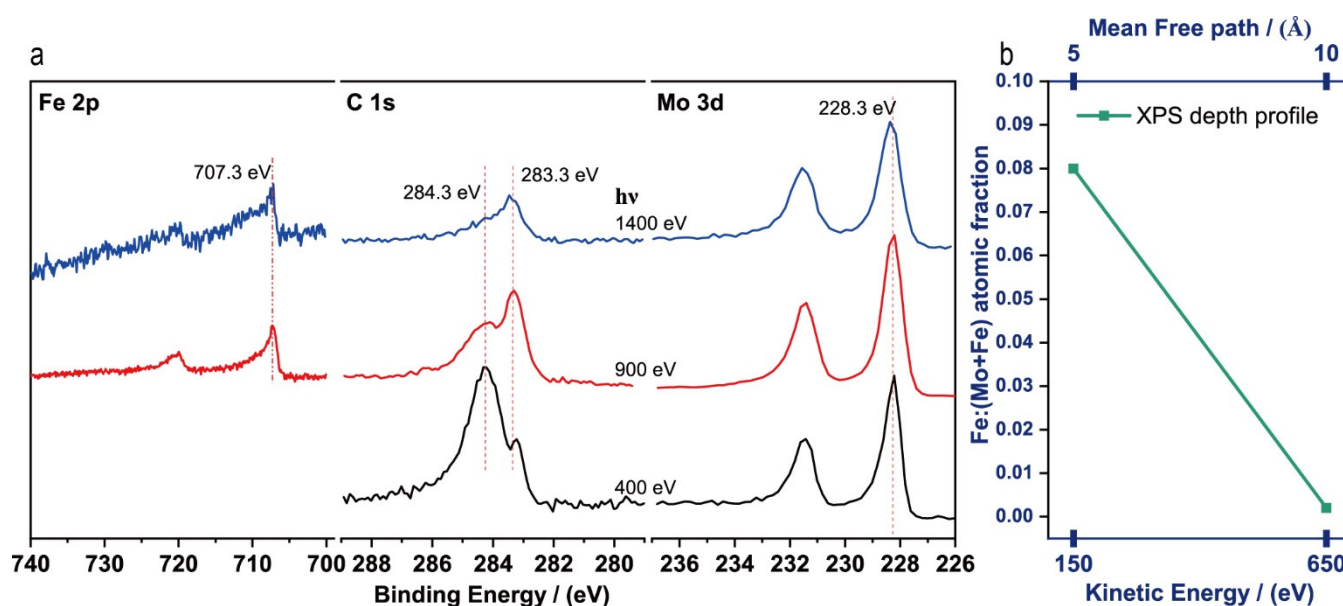


**Figure 4.** (a) Fe 2p, C 1s, and Mo 3d X-ray photoelectron spectroscopy (XPS) spectra of the prepared 1.5Fe-Mo<sub>2</sub>C-550 catalyst pretreated in a 20%CH<sub>4</sub>/H<sub>2</sub> atmosphere using a synchrotron-based XPS instrument with variable incident photon energies. (b) Dependence of Fe/(Fe + Mo) atomic fractions of as-synthesized 1.5Fe-Mo<sub>2</sub>C-550 catalyst measured using synchrotron-based XPS as a function of photoelectron kinetic energy and mean free path.

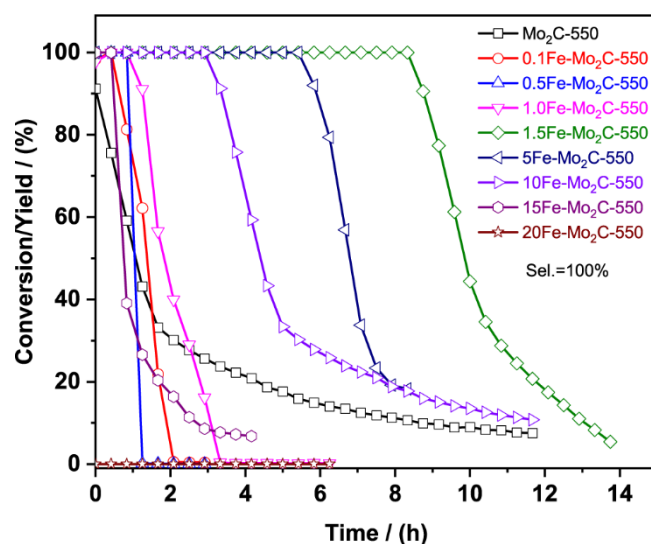
As indicated in Figure 4b, the measured atomic fraction Fe:(Mo + Fe) in the 1.5Fe-Mo<sub>2</sub>C-550 catalyst varied as a function of depth. The atomic fraction of Fe was 0.08 (~0.5 nm) near the surface of molybdenum carbide but dropped to 0.002 as the incident photon energy was increased to 1400 eV (~1 nm). Compared with the 0.015 Fe atomic fraction (Table S1) measured by ICP, we can confirm that well-dispersed Fe species should exist near the surface of the catalyst, not in the bulk. Supposedly, the modulated surface arising from the interaction between Mo<sub>2</sub>C and Fe might offer new active sites for toluene hydrogenation [54].

### 2.3. Fe-Mo<sub>2</sub>C Catalysts Performance

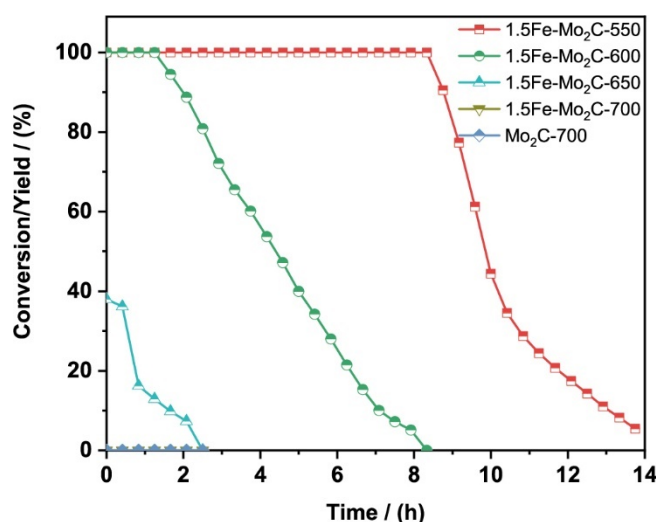
The effect of Fe loading on the catalytic performance of Fe-Mo<sub>2</sub>C catalysts for toluene hydrogenation is presented in Figure 5. Fe promotion substantially influences catalyst stability and activity. The unpromoted Mo<sub>2</sub>C-550 catalyst exhibited an initial activity of approximately 90% yield at 100 °C but quickly dropped to a conversion of 60% within one hour and reached 20% conversion after 4 h of reaction. Once a small amount of Fe was doped into Mo<sub>2</sub>C, the lifetime of the 1.5Fe-Mo<sub>2</sub>C-550 catalyst was substantially improved, as it maintained a 100% yield over 8.4 h, which is almost 10-fold longer than that of the non-doped catalyst. However, the higher doping amounts worsen the catalytic performance as the catalytic stability dramatically decreases with increasing Fe loadings. In particular, 15Fe-Mo<sub>2</sub>C-550 (15 at% Fe) showed a catalytic activity similar to that of unpromoted molybdenum carbide β-Mo<sub>2</sub>C, and 20Fe-Mo<sub>2</sub>C-550 displayed negligible activity for toluene hydrogenation [55,56]. The similarity between the initial activity of unpromoted Mo<sub>2</sub>C-550 catalyst and the promoted Mo<sub>2</sub>C with different Fe loadings suggests the Mo<sub>2</sub>C should be the real active sites for hydrogenation reaction, but the addition of the small amount of Fe largely inhibits the fast deactivation due to unknown reasons.

Figure 6 shows the effect of carburization temperature on the catalytic performance of Fe/Mo<sub>2</sub>C. The catalyst carburization temperature has a negative effect on the Fe/Mo<sub>2</sub>C catalyst performance. With increasing carburization temperature, the activities gradually decreased. The catalyst carburized at 600 °C displayed a poor initial activity, and the catalyst carburized at 700 °C was completely inactive for toluene hydrogenation. Clearly, the carburization temperature influences the particle sizes of the doped carbides (Figure 1b)

but does not change their crystalline structure. This finding means that for toluene hydrogenation, the defective surface of the doped carbide might display better catalytic activity than the well-crystallized surface. Considering the effect of Fe doping amounts on the catalytic performance, it suggests that surface defects in the Fe-modulated  $\text{Mo}_2\text{C}$  should be more active than the non-promoted  $\text{Mo}_2\text{C}$  and Fe nanoparticles. Moreover, the initial reactivity of  $\text{Mo}_2\text{C}$ -550 is quite close to that of the doped carbides, which suggests that the addition of Fe species does not substantially change the activity of active sites for toluene hydrogenation but inhibits rapid deactivation of the catalysts.



**Figure 5.** Effect of Fe doping amounts ( $x\text{Fe-Mo}_2\text{C-550}$ ,  $x = 0.1, 0.5, 1.0, 1.5, 5, 10, 15, 20$ ) on toluene hydrogenation. (3.0 MPa of total pressure, 100 °C as reaction temperature,  $0.15 \text{ h}^{-1}$  as WHSV, employing newly synthesized Fe-doped molybdenum carbide catalysts).



**Figure 6.** Effect of carburization temperature ( $1.5\text{Fe-Mo}_2\text{C-T}$ ,  $T = 550, 600, 650, 700 \text{ }^\circ\text{C}$ ) on toluene hydrogenation. (3.0 MPa of total pressure, 100 °C as reaction temperature,  $0.15 \text{ h}^{-1}$  as WHSV, employing newly synthesized Fe-doped molybdenum carbide catalysts).

We characterized fresh and spent  $1.5\text{Fe-Mo}_2\text{C-550}$  by XRD, TEM and XPS to study catalyst deactivation. No difference was observed between the XRD patterns of the fresh and used catalysts (Figure S5a), indicating the structural stability of the carbide catalyst in the toluene hydrogenation reaction. Microscopic evidence also confirms that the porous

microstructure of 1.5Fe-Mo<sub>2</sub>C-550 remained unchanged and that no segregation of Fe occurred after 14 h of the experiment (Figure 7 and Figure S5b,c). Although the Mo 3d and Fe 2p XPS spectra of fresh and used catalysts look similar, the O 1s XPS spectra show that after the reaction, a new peak at 532.7 eV appears, which should be assigned to OH species absorption on the surface of the catalyst (Figure 8) [57,58]. The XPS data suggest that surface oxidation might be the main reason for catalyst deactivation. Nevertheless, the C 1s XPS spectra also indicate that the surface of the fresh and used catalyst is still partially covered by graphitic carbon (Figure 8).

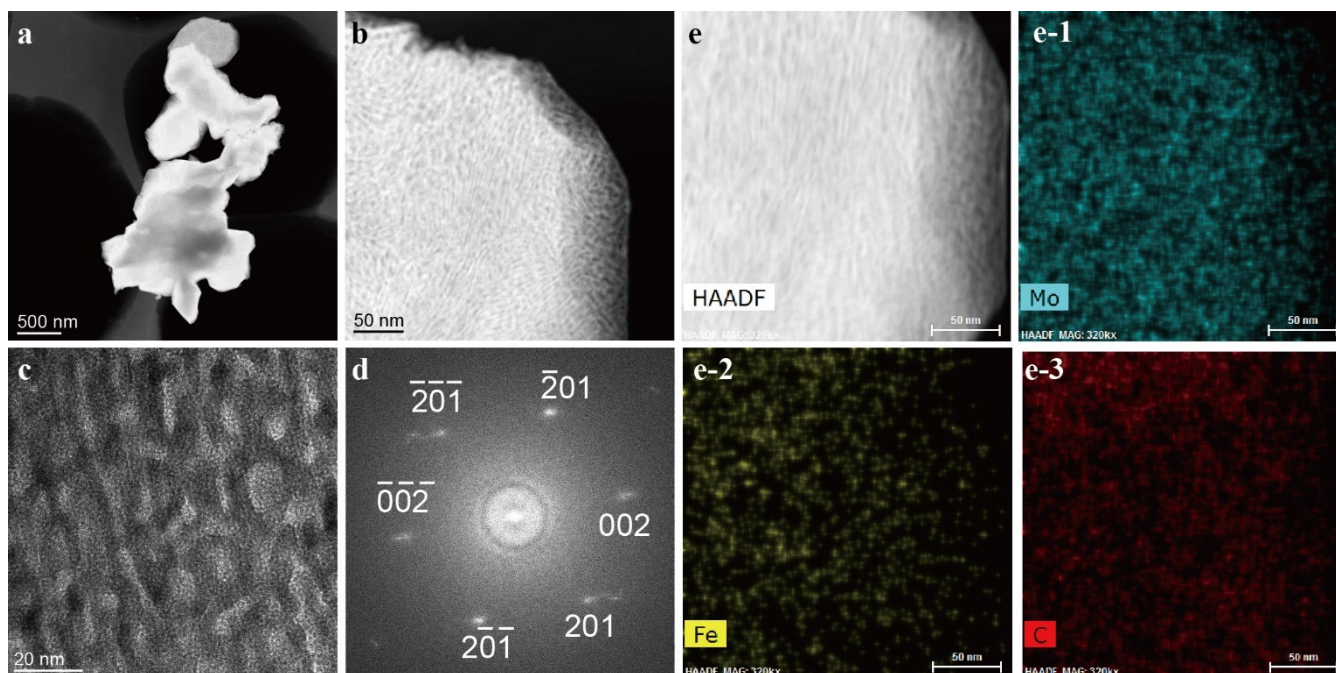


**Figure 7.** (a,b) STEM-HAADF image, (c,d) high-resolution TEM (HRTEM) image and its corresponding FFT image of spent 1.5Fe-Mo<sub>2</sub>C-550 catalyst, which show that its crystallinity and microstructure keep unchanged, (e) STEM-HAADF and its corresponding EDX element mapping of (e-1) Mo, (e-2) Fe, (e-3) C of spent catalyst 1.5Fe-Mo<sub>2</sub>C-550, indicating no aggregation of Fe species.

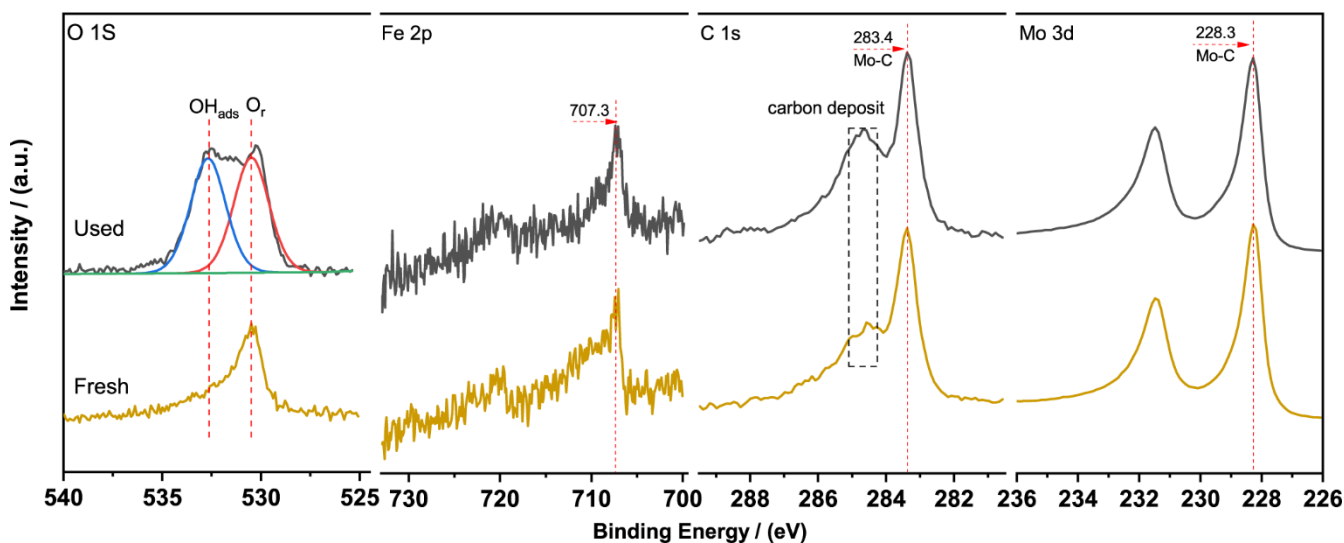


**Figure 8.** XPS spectra of fresh and spent catalysts of 1.5Fe-Mo<sub>2</sub>C-550 to study the change due to the reaction.

To distinguish the influences of surface oxidation and carbon deposition on catalyst activation, we recarburized the deactivated catalyst and tested its catalytic activity for the toluene hydrogenation reaction. As shown in Figure 9, the catalytic performance of the recarburized catalyst is fully recovered and displays identical catalytic performance to the fresh catalyst even after the third regeneration cycle. This result means that surface oxidation should be the main reason for catalyst deactivation. The addition of trace amounts of Fe might inhibit the adsorption of oxygen species in the hydrogenation process, which extends the lifetime of the carbide catalysts.

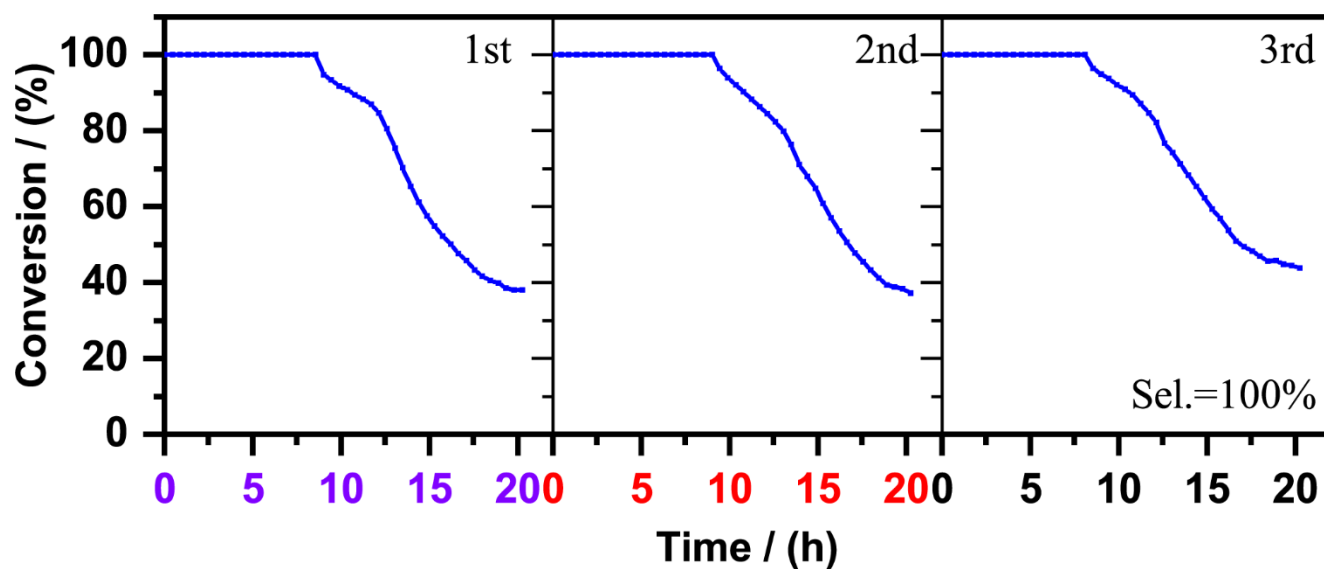


**Figure 9.** Catalyst 1.5Fe-Mo<sub>2</sub>C-550 reuse on toluene hydrogenation, 1st: after pretreatment, 2nd: regeneration after the first deactivation, 3rd: regeneration after the second deactivation. (The regeneration condition is the same as the pretreatment condition. Reaction conditions: 100 °C, WHSV: 0.15 h<sup>-1</sup>, pressure: 3 MPa).

### 3. Materials and Methods

#### 3.1. Synthetic Procedures

The Fe-MoO<sub>3</sub> precursors were synthesized by aqueous mixtures of iron nitrate (Fe(NO<sub>3</sub>)<sub>3</sub>·9H<sub>2</sub>O, 99%, Sigma-Aldrich, St. Louis, MO, USA) and ammonium molybdate tetrahydrate ((NH<sub>4</sub>)<sub>6</sub>Mo<sub>7</sub>O<sub>24</sub>·4H<sub>2</sub>O, 99%, Aladdin, Los Angeles, SC, USA), and the Fe atomic percent (at% (Fe/(Fe + Mo))) is 0.1 at%, 0.5 at%, 1.0 at%, 1.5 at%, 5 at%, 10 at%, 15 at%, 20 at%. The reagents were first dissolved in DI water at room temperature and the solution was stirred for 4 h and then transferred to rotary evaporator to dry the sample until no apparent moisture. After that, the solid sample was kept at 120 °C in an oven overnight and calcined in a muffle furnace at 500 °C for 4 h. The carburization of the precursor was carried out using home-made equipment, including gas controlling system and tube furnace for carburization which could be controlled by temperature-program. The precursor of Fe-MoO<sub>3</sub> was placed in quartz tube and both ends were plugged with silica wool. The quartz tube including precursor was put on tube furnace and then, in a 20% CH<sub>4</sub>/H<sub>2</sub> atmosphere, the temperature was increased from room temperature to 200 °C at 5 °C/min, and continuously increased to the final temperature (550 °C, 600 °C, 650 °C, 700 °C) at a rate of 1 °C/min. Finally, the reactor was cooled to room temperature to obtain the Fe-promoted molybdenum carbide (Fe-Mo<sub>2</sub>C) catalyst. For a contrast experiment, the MoO<sub>3</sub> precursor was synthesized by calcination of ammonium molybdate tetrahydrate at 500 °C for 4 h in a muffle furnace. Later, the MoO<sub>3</sub> was carburized in the same way as Fe-MoO<sub>3</sub>. In this work, the synthesized Fe-Mo<sub>2</sub>C catalyst with different Fe atomic percentages (0.1 at%, 0.5 at%, 1.0 at%, 1.5 at%, 5 at%, 10 at%, 15 at%, 20 at%) are denoted

as xFe-Mo<sub>2</sub>C-Y, in which X was 0.1, 0.5, 1.0, 1.5, 5, 10, 15, 20 and Y is 550, 600, 650 and 700, respectively.

### 3.2. Characterization

Brunauer–Emmett–Teller (BET) surface area analysis: the surface area was measured on a surface area analyzer (Model ASAP 2420, Micromeritics, Norcross, GA, USA) via nitrogen absorption at  $-196\text{ }^{\circ}\text{C}$  using the BET method.

X-ray diffraction (XRD) testing was performed on an X-ray diffractometer (Bruker D2 type, Karlsruhe, Germany). The test source was Cu K $\alpha$ , the test wavelength was 0.154 nm, the operating voltage and test current were 30 kV and 40 mA, respectively, and XRD patterns were recorded within a  $2\theta$  range of  $10\text{--}90^{\circ}$  with a scanning rate of  $4^{\circ}/\text{min}$ .

Temperature programmed carburization-reduction (TPC) was performed with home-made equipment [59]. Approximately 50 mg precursor was mounted in a quartz tube with an inner diameter of 6 mm, and a flow of 20% CH<sub>4</sub>/H<sub>2</sub> was used as the carburization-reduction gas. The precursor was first heated from  $20\text{ }^{\circ}\text{C}$  to  $200\text{ }^{\circ}\text{C}$  at a heating rate of  $10\text{ }^{\circ}\text{C}/\text{min}$  for 2 h in helium gas and then decreased to room temperature. After that, the gas was switched to 20% CH<sub>4</sub>/H<sub>2</sub> gas. The vent gas was detected by the measurement of the MS signal.

In situ XRD experiments were performed with a Bruker D8 Advance XRD equipped with a high-temperature reaction cell (SRK-900, Anton Paar GmbH, Graz, Austria). The sample temperature was increased from room temperature to  $700\text{ }^{\circ}\text{C}$  at a rate of  $1\text{ }^{\circ}\text{C}/\text{min}$ , and the carburization gas atmosphere was 20% CH<sub>4</sub>/H<sub>2</sub>. In situ XRD patterns were collected continuously with  $2\theta$  values ranging from  $10^{\circ}$  to  $80^{\circ}$  and a scanning rate of  $10^{\circ}/\text{min}$ .

X-ray photoelectron spectroscopy (XPS) was performed on an X-ray photoelectron spectrometer (Model: Thermo Scientific K-alpha, Waltham, MA, USA). The test source was Al K $\alpha$ , the instrument chamber pressure was  $1.0 \times 10^{-8}$  Pa, the test voltage was 1486.6 eV, and the electron beam pass energy was 50 eV. The test data were corrected to 283.4 eV (Mo-C). The instrument was equipped with a glove box to make the sample test avoid oxygen pollution as much as possible, and the test results were more accurate. The quasi in situ XPS was carried out in the following way: after carburization, the reactor was sealed under pure N<sub>2</sub> atmosphere and consecutively transferred to a glove box. The catalyst was pressed to a slice of 6 mm diameter in the glove box, and then the as-prepared sample was transferred to another glove box connected with an XPS load section using a sealed container avoiding the oxidation of the catalyst by air. After that, the sample was loaded, vacuumed to UHV and transferred to an analytic room for quasi in situ XPS characterization. The Figure S7 shows that the catalyst should not be oxidized during the transferring process.

Scanning electron microscopy (FEI Quanta 400 FEG type, Hillsboro, OR, USA) was used to observe and analyze the morphology of the sample. The test voltage was 15 kV, the magnification range was 20,000~240,000, and the objective lens distance during testing was 8.9 mm.

Scanning transmission electron microscopy (Thermo Fischer Talos F200X, Waltham, MA, USA) equipped with a Super-X EDX detector was operated with a acceleration voltage of 200 kV.

Inductively coupled plasma (ICP) analysis: The actual iron contents in the samples were determined by inductively coupled plasma-optical emission spectroscopy (ICP-OES) (Model Optima 2000, PerkinElmer, Waltham, MA, USA).

Ambient pressure X-ray photoelectron spectroscopy (APXPS): the APXPS experiments were measured at BL02B1 of the Shanghai Synchrotron Radiation Facility (SSRF). The bending magnet beamline delivers soft X-rays with a photon flux of approximately  $1 \times 10^{11}$  photons/s @  $E/\Delta E = 3700$  and a tightly focused beam spot size ( $\sim 200\text{ }\mu\text{m} \times 75\text{ }\mu\text{m}$ ) at the sample. All of the XPS spectra were calibrated by the Au 4f peak located at 84 eV (B.E.) [60].

### 3.3. Catalyst Test

The evaluation of the toluene hydrogenation reaction performance of the catalyst was performed on a fixed bed. The inner diameter of the fixed bed was 8 mm. The evaluation device consisted of three systems: a feed gas supply system, a reactor control system, and a product analysis system.

In the feed gas supply system, N<sub>2</sub> was divided into a balance gas for maintaining toluene as a gas and a carrier gas introducing saturated toluene vapor to the reactor, and H<sub>2</sub> was a reaction gas. Among them, H<sub>2</sub> was high-purity hydrogen, and N<sub>2</sub> was introduced into the reactor after dehydration, deoxidation, decarbonylation, and desulfurization. H<sub>2</sub> and the balance gas (N<sub>2</sub>) and carrier gas (N<sub>2</sub>) were controlled by a mass flow meter and connected to the reactor. The total gas flow rate was 50 mL/min, the carrier gas (N<sub>2</sub>) flow rate was 17.50 mL/min, the H<sub>2</sub> flow rate was 6.09 mL/min, the molar ratio of H<sub>2</sub>/toluene was 100, and the balance gas (N<sub>2</sub>) was 26.41 mL/min, which was for maintaining toluene gaseous state at 3 MPa. A small amount of gas at the outlet of the reactor was directly passed to the gas chromatograph for online analysis, and the remaining gas was discharged through the exhaust gas tube line. The reactor control system included three control systems: pressure, temperature and flow. The pipeline gas entered the reactor through the pressure-reducing valve, and the reaction pressure was controlled at 3 MPa. The temperature control system was controlled by a temperature controller produced by the Shanxi Institute of Coal Chemistry, Chinese Academy of Sciences.

To calculate conversion and selectivity values, a gas chromatograph couple was connected to the reactor system. The GC System (Agilent 7890B, Santa Clara, CA, America) equipped with an PONA column with the following parameters: length: 50 m, inner diameter: 200 µm, and film thickness of 0.5 µm, and a flame ionization detector (FID) was used to analyze the online gas stream. The separation of these products was achieved by the following temperature program: 40 °C as the initial temperature (holding for 12 min), ramp: 3 °C/min up to 70 °C.

Toluene hydrogenation was used as probe reaction to determine the hydrogenation performance of the catalysts. Before the reaction measurements, the catalysts were pre-treated in 20% CH<sub>4</sub>/H<sub>2</sub> at 100 mL/min at 550 °C for 2 h (heating rate from RT of 2 °C/min). Afterward, the temperature was directly decreased to the reaction temperature. The hydrogenation of toluene was performed at two temperatures (80 °C and 100 °C) and 30 bar. A flow of N<sub>2</sub> was passed through two toluene saturators in series maintained at 80 °C and 50 °C to obtain stable toluene vapor. The products were analyzed by an online GC-7890B.

## 4. Conclusions

We found that the catalytic performances of the molybdenum carbide catalysts for toluene hydrogenation could be effectively modulated by adding cheap transition metals like Fe. The crystalline characteristics and microstructure of the Fe-doped molybdenum carbide characterized by XRD and TEM show that the addition of Fe promotes the carburization process but does not change their crystalline properties. Synchrotron-based XPS and STEM-EDX element mapping data suggest Fe species are highly dispersive but accumulated in the surface of the synthetic catalyst. The addition of the small amount of Fe slightly changes the initial activity of the molybdenum carbide catalysts, but strongly promote their catalytic stability. The deactivation should be attributed to the surface oxidation but the re-carburization treatment can fully recover their catalytic activity to toluene hydrogenation.

**Supplementary Materials:** The following are available online at <https://www.mdpi.com/article/10.3390/catal11091079/s1>, Table S1: Textural properties and elemental compositions of the as-prepared Fe-Mo<sub>2</sub>C catalysts with different Fe loadings, Figure S1: (a) XRD patterns of beta-Mo<sub>2</sub>C prepared at different final temperatures (550 °C, 600 °C, 630 °C, 650 °C and 700 °C), (b) XRD patterns of Fe-MoO<sub>3</sub> precursors, Figure S2: SEM images of (a) MoO<sub>3</sub>, (b) beta-Mo<sub>2</sub>C, (c) 1.5Fe-MoO<sub>3</sub>, (d) 1.5Fe-Mo<sub>2</sub>C-550, (e) 10Fe-MoO<sub>3</sub>, (f) 10Fe-Mo<sub>2</sub>C-550, Figure S3: Temperature-programmed carburization of Fe-MoO<sub>3</sub> and using MS to detect the vent gas of H<sub>2</sub>O (m/z = 18) and CO (m/z = 28), Figure S4:

STEM image and corresponding element mapping picture of 1.5Fe-Mo<sub>2</sub>C-550, Figure S5: (a) XRD patterns of catalyst (1.5Fe-Mo<sub>2</sub>C-600) before and after the reaction, (b) SEM image of spent catalyst (1.5Fe-Mo<sub>2</sub>C-550), (c) STEM-HAADF image of spent catalyst (1.5Fe-Mo<sub>2</sub>C-550), and (d) STEM image and corresponding STEM-EDX element mapping image of spent catalyst (1.5Fe-Mo<sub>2</sub>C-550). Figure S6: Carbon balance curve of during toluene hydrogenation using 1.5Fe-Mo<sub>2</sub>C-550 as catalyst. (3.0 MPa of total pressure, 100 °C as reaction temperature, 0.15 h<sup>-1</sup> as WHSV, employing newly synthesized Fe-doped molybdenum carbide catalysts). Figure S7: A control experiment using catalyst of 1.5Fe-Mo<sub>2</sub>C-550 for examining if surface of molybdenum carbide should be oxidized during transferring. The 1.5Fe-MoO<sub>3</sub> precursor was carburized in a fixed bed, which is identical one to the equipment used in toluene hydrogenation, at an atmosphere of 20% CH<sub>4</sub>/H<sub>2</sub>. After carburization, the reactor was sealed under pure N<sub>2</sub> atmosphere and consecutively transferred to glove box. The catalyst was pressed to a slice of 6 mm diameter in the glove box, and then the as-prepared sample was transferred to another glove box connected with XPS equipment load section using a sealed container avoiding the oxidation of catalyst by air. After that, the sample was loaded, vacuumed to UHV and transferred to analytical room for quasi in-situ XPS characterization.

**Author Contributions:** Conceptualization, X.L. (Xi Liu) and J.X.; formal analysis, S.Z.; APXPS, H.Z. and X.L. (Xiaosong Liu); investigation, S.Z. and P.L.; writing—original draft preparation, S.Z.; writing—review and editing, X.L. (Xi Liu) and J.X.; supervision, X.L. (Xi Liu) and J.X.; project administration, X.W. and Y.Y.; funding acquisition, Y.L. All authors have read and agreed to the published version of the manuscript.

**Funding:** This work was supported by the National Science Foundation of China (No. 21872163 and 22072090) and supported from the “transformational technologies for clean energy and demonstration”, strategic priority research program of Chinese Academy of Sciences, Grant No. XDA 21000000.

**Data Availability Statement:** This study did not report any data.

**Acknowledgments:** The authors are grateful for the facilities and financial support from Synfuels China Co. Ltd. and the authors also thank BL02B01 of the Shanghai Synchrotron Radiation Facility, supported by the National Science Foundation of China under contract No. 11227902. The innovation foundation of the Institute of Coal Chemistry, Chinese Academy of Sciences, is also gratefully acknowledged.

**Conflicts of Interest:** The authors declare no conflict of interest.

## References

1. Yang, H.; Xue, N.; Liu, X. High-Strength Porous Millimeter Carbon Ball Having Controllable Internal Structure Useful in Fixed Bed Reactor for Catalytic Hydrogenation Reaction System. Patent CN112028050-A, 4 December 2020.
2. Niu, M.; Tian, R.; Fan, Z.; Ji, P. Preparation of Gasoline and Diesel Oil by Mixing Coal Tar with Biomass Oil, Performing Catalytic Hydrogenation, Rectifying to Obtain Gasoline and Diesel Oil Product, and Using Coal Tar as Hydrogen Supply Solvent for Hydrogen Free Radical. Patent CN112029532-A, 4 December 2020.
3. Cacciola, G.; Giordano, N.; Restuccia, G. Cyclohexane as a liquid phase carrier in hydrogen storage and transport. *Int. J. Hydrog. Energy* **1984**, *9*, 411–419. [[CrossRef](#)]
4. Hamayun, M.H.; Maafa, I.M.; Hussain, M.; Aslam, R. Simulation Study to Investigate the Effects of Operational Conditions on Methylcyclohexane Dehydrogenation for Hydrogen Production. *Energies* **2020**, *13*, 206. [[CrossRef](#)]
5. Gong, Y.; Yuan, Y.; Chen, C.; Chaemchuen, S.; Verpoort, F. Palladium metallated shell layer of shell@core MOFs as an example of an efficient catalyst design strategy for effective olefin hydrogenation reaction. *J. Catal.* **2020**, *392*, 141–149. [[CrossRef](#)]
6. Peyrovi, M.H.; Rostamikia, T.; Parsafard, N. Competitive Hydrogenation of Benzene in Reformate Gasoline over Ni Supported on SiO<sub>2</sub>, SiO<sub>2</sub>-Al<sub>2</sub>O<sub>3</sub>, and Al<sub>2</sub>O<sub>3</sub> Catalysts: Influence of Support Nature. *Energy Fuels* **2018**, *32*, 11432–11439. [[CrossRef](#)]
7. Weillhard, A.; Abarca, G.; Viscardi, J.; Precht, M.H.G.; Scholten, J.D.; Bernardi, F.; Baptista, D.L.; Dupont, J. Challenging Thermodynamics: Hydrogenation of Benzene to 1,3-Cyclohexadiene by Ru@Pt Nanoparticles. *ChemCatChem* **2017**, *9*, 204–211. [[CrossRef](#)]
8. Bi, H.; Tan, X.; Dou, R.; Pei, Y.; Qiao, M.; Sun, B.; Zong, B. Ru-B nanoparticles on metal-organic frameworks as excellent catalysts for hydrogenation of benzene to cyclohexane under mild reaction conditions. *Green Chem.* **2016**, *18*, 2216–2221. [[CrossRef](#)]
9. Foppa, L.; Dupont, J. Benzene partial hydrogenation: Advances and perspectives. *Chem. Soc. Rev.* **2015**, *44*, 1886–1897. [[CrossRef](#)]
10. Cai, J.; Bennici, S.; Shen, J.; Auroux, A. Influence of N addition in mesoporous carbons used as supports of Pt, Pd and Ru for toluene hydrogenation and iron oxide for benzene oxidation. *React. Kinet. Mech. Catal.* **2015**, *115*, 263–282. [[CrossRef](#)]
11. Sun, H.; Guo, W.; Zhou, X.; Chen, Z.; Liu, Z.; Liu, S. Progress in Ru-Based Amorphous Alloy Catalysts for Selective Hydrogenation of Benzene to Cyclohexene. *Chin. J. Catal.* **2011**, *32*, 1–16. [[CrossRef](#)]

12. Kazantsev, R.V.; Gaidai, N.A.; Nekrasov, N.V.; Tenchev, K.; Petrov, L.; Lapidus, A.L. Kinetics of benzene and toluene hydrogenation on a Pt/TiO<sub>2</sub> catalyst. *Kinet. Catal.* **2003**, *44*, 529–535. [[CrossRef](#)]
13. Yang, Y.; Liu, X.; Xu, Y.; Gao, X.; Dai, Y.; Tang, Y. Palladium-Incorporated  $\alpha$ -MoC Mesoporous Composites for Enhanced Direct Hydrodeoxygenation of Anisole. *Catalysts* **2021**, *11*, 370. [[CrossRef](#)]
14. Mamède, A.; Giraudon, J.-M.; Löfberg, A.; Leclercq, L. Hydrogenation of toluene over  $\beta$ -Mo<sub>2</sub>C in the presence of thiophene. *Appl. Catal. A-Gen.* **2002**, *227*, 73–82. [[CrossRef](#)]
15. Da Costa, P.; Lemberton, J.-L.; Potvin, C.; Manoli, J.-M.; Perot, G.; Breyse, M.; Djéga-Mariadassou, G. Tetralin hydrogenation catalyzed by Mo<sub>2</sub>C/Al<sub>2</sub>O<sub>3</sub> and WC/Al<sub>2</sub>O<sub>3</sub> in the presence of H<sub>2</sub>S. *Catal. Today* **2001**, *65*, 195–200. [[CrossRef](#)]
16. Lin, S.D.; Song, C. Noble metal catalysts for low-temperature naphthalene hydrogenation in the presence of benzothiophene. *Catal. Today* **1996**, *31*, 93–104. [[CrossRef](#)]
17. Stanislaus, A.; Cooper, B.H. Aromatic Hydrogenation Catalysis: A Review. *Catal. Rev.* **1994**, *36*, 75–123. [[CrossRef](#)]
18. Murugesan, K.; Senthamarai, T.; Alshammari, A.S.; Altamimi, R.M.; Kreyenschulte, C.; Pohl, M.M.; Lund, H.; Jagadeesh, R.V.; Beller, M. Cobalt-Nanoparticles Catalyzed Efficient and Selective Hydrogenation of Aromatic Hydrocarbons. *ACS Catal.* **2019**, *9*, 8581–8591. [[CrossRef](#)]
19. Peyrovi, M.; Parsafard, N.; Mohammadian, Z. Benzene selective hydrogenation over supported Ni (nano-) particles catalysts: Catalytic and kinetics studies. *Chin. J. Chem. Eng.* **2018**, *26*, 521–528. [[CrossRef](#)]
20. Wei, Q.; Chen, J.; Song, C.; Li, G. HDS of dibenzothiophenes and hydrogenation of tetralin over a SiO<sub>2</sub> supported Ni-Mo-S catalyst. *Front. Chem. Sci. Eng.* **2015**, *9*, 336–348. [[CrossRef](#)]
21. Wang, W.; Li, L.; Wu, K.; Zhang, K.; Jie, J.; Yang, Y. Preparation of Ni-Mo-S catalysts by hydrothermal method and their hydrodeoxygenation properties. *Appl. Catal. A-Gen.* **2015**, *495*, 8–16. [[CrossRef](#)]
22. Schachtl, E.; Zhong, L.; Kondratieva, E.; Hein, J.; Gutiérrez, O.Y.; Jentys, A.; Lercher, J.A. Understanding Ni Promotion of MoS<sub>2</sub>/-Al<sub>2</sub>O<sub>3</sub> and its Implications for the Hydrogenation of Phenanthrene. *ChemCatChem* **2015**, *7*, 4118–4130. [[CrossRef](#)]
23. Wang, W.; Zhang, K.; Li, L.; Wu, K.; Liu, P.; Yang, Y. Synthesis of Highly Active Co-Mo-S Unsupported Catalysts by a One-Step Hydrothermal Method for p-Cresol Hydrodeoxygenation. *Ind. Eng. Chem. Res.* **2014**, *53*, 19001–19009. [[CrossRef](#)]
24. Gutiérrez, O.Y.; Singh, S.; Schachtl, E.; Kim, J.; Kondratieva, E.; Hein, J.; Lercher, J. Effects of the Support on the Performance and Promotion of (Ni)MoS<sub>2</sub> Catalysts for Simultaneous Hydrodenitrogenation and Hydrodesulfurization. *ACS Catal.* **2014**, *4*, 1487–1499. [[CrossRef](#)]
25. Choi, J.; Barnard, Z.G.; Zhang, S.; Hill, J.M. Ni catalysts supported on activated carbon from petcoke and their activity for toluene hydrogenation. *Can. J. Chem. Eng.* **2012**, *90*, 631–636. [[CrossRef](#)]
26. Cho, A.; Moon, S.H. Development of Highly Active Co(Ni)Mo Catalysts for the Hydrodesulfurization of Dibenzothiophene Compounds. *Catal. Surv. Asia* **2010**, *14*, 64–74. [[CrossRef](#)]
27. Moses, P.G.; Hinnemann, B.; Topsøe, H.; Nørskov, J.K. The effect of Co-promotion on MoS<sub>2</sub> catalysts for hydrodesulfurization of thiophene: A density functional study. *J. Catal.* **2009**, *268*, 201–208. [[CrossRef](#)]
28. Xiao, T.C.; York, A.P.; Megren, H.A.; Williams, C.V.; Wang, H.T.; Green, M.L. Preparation and characterisation of bimetallic cobalt and molybdenum carbides. *J. Catal.* **2001**, *202*, 100–109. [[CrossRef](#)]
29. Dhandapani, B.; Clair, T.S.; Oyama, S. Simultaneous hydrodesulfurization, hydrodeoxygenation, and hydrogenation with molybdenum carbide. *Appl. Catal. A-Gen.* **1998**, *168*, 219–228. [[CrossRef](#)]
30. Yao, S.; Zhang, X.; Zhou, W.; Gao, R.; Xu, W.; Ye, Y.; Lin, L.; Wen, X.; Liu, P.; Chen, B.; et al. Atomic-layered Au clusters on  $\alpha$ -MoC as catalysts for the low-temperature water-gas shift reaction. *Science* **2017**, *357*, 389–393. [[CrossRef](#)] [[PubMed](#)]
31. Liu, Y.; Zhu, X.; Zhang, Q.-H.; Tang, T.; Zhang, Y.; Gu, L.; Li, Y.; Bao, J.; Dai, Z.; Hu, J.-S. Engineering Mo/Mo<sub>2</sub>C/MoC hetero-interfaces for enhanced electrocatalytic nitrogen reduction. *J. Mater. Chem. A* **2020**, *8*, 8920–8926. [[CrossRef](#)]
32. Kojima, R.; Aika, K.-I. Molybdenum nitride and carbide catalysts for ammonia synthesis. *Appl. Catal. A-Gen.* **2001**, *219*, 141–147. [[CrossRef](#)]
33. Zhang, X.; Zhu, X.; Lin, L.; Yao, S.; Zhang, M.; Liu, X.; Wang, X.; Li, Y.W.; Shi, C.; Ma, D. Highly Dispersed Copper over  $\beta$ -Mo<sub>2</sub>C as an Efficient and Stable Catalyst for the Reverse Water Gas Shift (RWGS) Reaction. *ACS Catal.* **2016**, *7*, 912–918. [[CrossRef](#)]
34. Xu, W.; Ramirez, P.J.; Stacchiola, D.; Rodriguez, J.A. Synthesis of  $\alpha$ -MoC<sub>1-x</sub> and  $\beta$ -MoC<sub>y</sub> Catalysts for CO<sub>2</sub> Hydrogenation by Thermal Carburization of Mo-oxide in Hydrocarbon and Hydrogen Mixtures. *Catal. Lett.* **2014**, *144*, 1418–1424. [[CrossRef](#)]
35. Dongil, A.B.; Zhang, Q.; Pastor-Pérez, L.; Ramírez-Reina, T.; Guerrero-Ruiz, A.; Rodríguez-Ramos, I. Effect of Cu and Cs in the  $\beta$ -Mo<sub>2</sub>C System for CO<sub>2</sub> Hydrogenation to Methanol. *Catalysts* **2020**, *10*, 1213. [[CrossRef](#)]
36. Shilov, I.N.; Smirnov, A.A.; Bulavchenko, O.A.; Yakovlev, V.A. Effect of Ni–Mo Carbide Catalyst Formation on Furfural Hydrogenation. *Catalysts* **2018**, *8*, 560. [[CrossRef](#)]
37. Rodriguez, J.A.; Liu, P.; Takahashi, Y.; Nakamura, K.; Viñes, F.; Illas, F. Desulfurization Reactions on Surfaces of Metal Carbides: Photoemission and Density-Functional Studies. *Top. Catal.* **2010**, *53*, 393–402. [[CrossRef](#)]
38. Piskorz, W.; Adamski, G.; Kotarba, A.; Sojka, Z.; Sayag, C.; Djéga-Mariadassou, G. Hydrodenitrogenation of indole over Mo<sub>2</sub>C catalyst: Insights into mechanistic events through DFT modeling. *Catal. Today* **2007**, *119*, 39–43. [[CrossRef](#)]
39. Diaz, B.; Sawhill, S.J.; Bale, D.H.; Main, R.; Phillips, D.C.; Korlann, S.; Self, R.; Bussell, M.E. Hydrodesulfurization over supported monometallic, bimetallic and promoted carbide and nitride catalysts. *Catal. Today* **2003**, *86*, 191–209. [[CrossRef](#)]
40. Lewandowski, M.; Janus, R.; Wądrzyk, M.; Szymańska-Kolasa, A.; Sayag, C.; Djéga-Mariadassou, G. On Catalytic Behavior of Bulk Mo<sub>2</sub>C in the Hydrodenitrogenation of Indole over a Wide Range of Conversion Thereof. *Catalysts* **2020**, *10*, 1355. [[CrossRef](#)]

41. Deng, Y.; Ge, Y.; Xu, M.; Yu, Q.; Xiao, D.; Yao, S.; Ma, D. Molybdenum Carbide: Controlling the Geometric and Electronic Structure of Noble Metals for the Activation of O–H and C–H Bonds. *Acc. Chem. Res.* **2019**, *52*, 3372–3383. [[CrossRef](#)]
42. Lin, L.; Yu, Q.; Peng, M.; Li, A.; Yao, S.; Tian, S.; Liu, X.; Li, A.; Jiang, Z.; Gao, R.; et al. Atomically Dispersed Ni/ $\alpha$ -MoC Catalyst for Hydrogen Production from Methanol/Water. *J. Am. Chem. Soc.* **2020**, *143*, 309–317. [[CrossRef](#)]
43. Lin, L.; Zhou, W.; Gao, R.; Yao, S.; Zhang, X.; Xu, W.; Zheng, S.; Jiang, Z.; Yu, Q.; Li, Y.-W.; et al. Low-temperature hydrogen production from water and methanol using Pt/ $\alpha$ -MoC catalysts. *Nature* **2017**, *544*, 80–83. [[CrossRef](#)] [[PubMed](#)]
44. Raghav, H.; Konathala, L.S.K.; Mishra, N.; Joshi, B.; Goyal, R.; Agrawal, A.; Sarkar, B. Fe-decorated hierarchical molybdenum carbide for direct conversion of CO<sub>2</sub> into ethylene: Tailoring activity and stability. *J. CO<sub>2</sub> Util.* **2021**, *50*, 101607. [[CrossRef](#)]
45. Koverga, A.A.; Gómez-Marín, A.M.; Dorkis, L.; Florez, E.; Ticianelli, E.A. Role of Transition Metals on TM/Mo<sub>2</sub>C Composites: Hydrogen Evolution Activity in Mildly Acidic and Alkaline Media. *ACS Appl. Mater. Interfaces* **2020**, *12*, 27150–27165. [[CrossRef](#)] [[PubMed](#)]
46. Xiang, M.; Zou, J. CO Hydrogenation over Transition Metals (Fe, Co, or Ni) Modified K/Mo<sub>2</sub>C Catalysts. *J. Catal.* **2013**, *2013*, 195920. [[CrossRef](#)]
47. Suppino, R.S.; Landers, R.; Cobo, A.J.G. Effects of the activation method on the performance of base metal catalysts prepared by wet impregnation for toluene hydrogenation in liquid phase. *React. Kinet. Mech. Catal.* **2015**, *114*, 295–309. [[CrossRef](#)]
48. Yoon, K.J.; Vannice, M.A. Benzene hydrogenation over iron: II. Reaction model over unsupported and supported catalysts. *J. Catal.* **1983**, *82*, 457–468. [[CrossRef](#)]
49. Ma, Y.; Guan, G.; Hao, X.; Zuo, Z.; Huang, W.; Phanthong, P.; Kusakabe, K.; Abudula, A. Highly-efficient steam reforming of methanol over copper modified molybdenum carbide. *RSC Adv.* **2014**, *4*, 44175–44184. [[CrossRef](#)]
50. Alayoglu, S.; Somorjai, G.A. Ambient Pressure X-ray Photoelectron Spectroscopy for Probing Monometallic, Bimetallic and Oxide-Metal Catalysts Under Reactive Atmospheres and Catalytic Reaction Conditions. *Top. Catal.* **2016**, *59*, 420–438. [[CrossRef](#)]
51. Tao, F.; Grass, M.E.; Zhang, Y.; Butcher, D.R.; Renzas, J.R.; Liu, Z.; Chung, J.Y.; Mun, B.S.; Salmeron, M.; Somorjai, G.A. Reaction-Driven Restructuring of Rh-Pd and Pt-Pd Core-Shell Nanoparticles. *Science* **2008**, *322*, 932–934. [[CrossRef](#)]
52. Powell, C.J.; Jablonski, A.; Salvat, F. NIST databases with electron elastic-scattering cross sections, inelastic mean free paths, and effective attenuation lengths. *Surf. Interface Anal.* **2005**, *37*, 1068–1071. [[CrossRef](#)]
53. Idczak, K.; Idczak, R. Investigation of Surface Segregation in Fe-Cr-Si Alloys by XPS. *Met. Mater. Trans. A* **2020**, *51*, 3076–3089. [[CrossRef](#)]
54. Yao, S.; Lin, L.; Liao, W.; Rui, N.; Li, N.; Liu, Z.; Cen, J.; Zhang, F.; Li, X.; Song, L.; et al. Exploring Metal-Support Interactions To Immobilize Subnanometer Co Clusters on  $\gamma$ -Mo<sub>2</sub>N: A Highly Selective and Stable Catalyst for CO<sub>2</sub> Activation. *ACS Catal.* **2019**, *9*, 9087–9097. [[CrossRef](#)]
55. Frauwallner, M.-L.; López-Linares, F.; Lara-Romero, J.; Scott, C.E.; Ali, V.; Hernández, E.; Pereira-Almao, P. Toluene hydrogenation at low temperature using a molybdenum carbide catalyst. *Appl. Catal. A-Gen.* **2011**, *394*, 62–70. [[CrossRef](#)]
56. Lee, J.S.; Yeom, M.H.; Park, K.Y.; Nam, I.-S.; Chung, J.S.; Kim, Y.G.; Moon, S.H. Preparation and benzene hydrogenation activity of supported molybdenum carbide catalysts. *J. Catal.* **1991**, *128*, 126–136. [[CrossRef](#)]
57. Zhang, X.; Zhang, M.; Deng, Y.; Xu, M.; Artiglia, L.; Wen, W.; Gao, R.; Chen, B.; Yao, S.; Zhang, X.; et al. A stable low-temperature H<sub>2</sub>-production catalyst by crowding Pt on  $\alpha$ -MoC. *Nature* **2021**, *589*, 396–401. [[CrossRef](#)] [[PubMed](#)]
58. Mudiyansele, K.; Senanayake, S.; Feria, L.; Kundu, S.; Baber, A.E.; Graciani, J.; Vidal, A.B.; Agnoli, S.; Evans, J.; Chang, R.; et al. Importance of the Metal-Oxide Interface in Catalysis: In Situ Studies of the Water-Gas Shift Reaction by Ambient-Pressure X-ray Photoelectron Spectroscopy. *Angew. Chem. Int. Ed.* **2013**, *52*, 5101–5105. [[CrossRef](#)] [[PubMed](#)]
59. Xu, J.; Bartholomew, C.H. Temperature-Programmed Hydrogenation (TPH) and in Situ Mössbauer Spectroscopy Studies of Carbonaceous Species on Silica-Supported Iron Fischer–Tropsch Catalysts. *J. Phys. Chem. B* **2005**, *109*, 2392–2403. [[CrossRef](#)] [[PubMed](#)]
60. Cai, J.; Dong, Q.; Han, Y.; Mao, B.-H.; Zhang, H.; Karlsson, P.G.; Åhlund, J.; Tai, R.-Z.; Yu, Y.; Liu, Z. An APXPS endstation for gas–solid and liquid–solid interface studies at SSRF. *Nucl. Sci. Tech.* **2019**, *30*, 81. [[CrossRef](#)]